Energy and Exergy Analysis of Internal Combustion Engine Performance of Spark Ignition for Gasoline, Methane, and Hydrogen Fuels

Norouzi, Nima
Department of Energy Engineering and Physics, Amirkabir University of Technology, PO. Box 15875-4413, Tehran, I.R. IRAN

Ebadi, Abdol Ghaffar
Department of Agriculture, Jouybar Branch, Islamic Azad University, Jouybar, I.R. IRAN

Bozorgian, Ali Reza*[+]
Department of Chemical Engineering, Mahshahr Branch, Islamic Azad University, Mahshahr, I.R. IRAN

Hoseyni, Seyed Jalal
Department of Chemistry, Shams Gonbad Higher Education Institute, Gonbad Kavous, I.R. IRAN

Vessally, Esmail
Department of Chemistry, Payame Noor University, I.R. IRAN

ABSTRACT: *Exergy analysis is a tool to determine the share of processes involved in transferring input functionality to the system and where the useful energy loss occurs in a system or process. In this study, an exergy comparison of the performance of an internal combustion engine with spark-ignition for gasoline, hydrogen, and methane fuels is considered. For this purpose, first, multi-zone modeling of the engine based on flame advancement has been introduced. Then, the necessary conceptual bases for performing exergy analysis of the system have been established by defining the term exergy and creating the corresponding exergy balance equations and applying them to closed systems and control volumes. This study shows that the largest share of irreversibility in the engine is related to the combustion process. Also, for stoichiometric conditions, we can mention the percentage of exergy transferred by working approximately equal for all three fuels, the highest percentage of irreversibility for gasoline, and the lowest percentage of irreversibility for hydrogen. Examining the exergy analysis results in the assumed operating conditions mentioned in the paper shows that increasing engine speed increases exergy transfer with work and decreases exergy transfer with heat. Also, increasing the equivalence ratio increases the share of exergy of the mixture inside the cylinder and decreases the irreversible share of inlet exergy.*

KEYWORDS: *Internal combustion engine; Multi-zone simulation; Exergy analysis; Alternative fuels.*

***** *To whom correspondence should be addressed.*
+ E-mail: *a.bozorgian@mhriau.ac.ir*
1021-9986/2021/6/1909-1930 *22/$/7.02*

INTRODUCTION

Nearly half a century ago, models of internal combustion engines were developed to predict the pressure, temperature, and composition of gases in the cylinder in terms of time or crank angle. The first combustion models were obtained by applying the first law of thermodynamics to a closed system with a time-dependent volume as a single zone (zero-dimensional model) [1]. The assumption of instantaneous mixing between the burned and unburned gases leads to a uniform distribution of properties in the combustion chamber, is unrealistic. To overcome this inaccurate assumption, multivariate models were developed. In these models, the cylinder mixture is divided into burnt, unburned, and ready-to-burn areas, and it is assumed that the temperature and composition of the gases are uniform in each of these areas and that the pressure is instantly uniform throughout the chamber. In these models, the amount of unburned mixture that burns at any crank angle is determined by the speed and radius of the flame front [2-10]. Quasi-dimensional models calculate the properties of the combustion chamber only in terms of time or crank angle, and in the divided regions of the chamber, consider the mixture uniform and are based on the laws of mass conservation and energy conservation[11-20].

As mentioned, in the conventional multidimensional models of the mass conservation balance and the first law of thermodynamics, the second law of thermodynamics is not considered one of the modeling parts. However, with the development of thermodynamic concepts, it became clear that the first law does not fully determine the engine's performance. The second law needs to investigate the exergy destruction and irreversibility level that can be used in various engine processes. Thus, the exergy analysis of engine processes to identify the areas of declining efficiency became common [4,5]. For more than 40 years, articles and reports have been published using the second law of thermodynamics to analyze diesel and gasoline engines' performance and related subsystems.

Meanwhile, the use of exergy analysis to compare engine performance with alternative fuels is a major part. *Azoumah et al.* [6] investigated the performance of compression combustion engines with biofuels by the first and second laws of thermodynamics. Also, from this perspective, the analysis of the transient behavior of internal combustion engines has been considered. *Nieminen* and *Dincer* [7] have compared the exergy performance of gasoline and hydrogen spark-ignition engines and thus obtained various factors in transmitting input exergy. A complete example of energy analysis and exergy application on the internal combustion engine is an article by *Mahabadipour et al.* [8]. Also, in this study, subsystems such as superchargers on engine performance have been studied.

In a study by *Dogan et al.* [9, 10], ethanol which has high octane rating, low exhaust emission, and which is easily obtained from agricultural products, has been used in fuels prepared by blending it with gasoline in various ratios (E0, E10, E20, and E30). Ethanol-gasoline blends have been used in a four-cylinder four-stroke spark-ignition engine for performance and emission analysis under full load. The experimental studies measured engine torque, fuel, and cooling water flow rates, and exhaust and engine surface temperature. Engine energy distribution, irreversible processes in the cooling system and the exhaust, and the exergy distribution have been calculated using the experimental data and the formulas for the first and second laws of thermodynamics. Experiments and theoretical calculations showed that ethanol-added fuels show a reduction in carbon monoxide (CO), carbon dioxide (CO_2), and nitrogen oxide (NO_X) emissions without significant loss of power compared to gasoline. Nevertheless, it was measured that reducing the temperature inside the cylinder increases the hydrocarbon (HC) emission.

In a study by *Dhyani* and *Subramanian* [11], an experimental investigation was carried out on a multi-cylinder spark ignition (SI) engine fuelled with compressed natural gas (CNG), hydrogen blended CNG (HCNG), and hydrogen with varying load at 1500 rpm in order to perform comparative exergy analysis. The exergy analysis indicates that work exergy, heat transfer exergy, and exhaust exergy were the highest with hydrogen at all loads due to its high flame temperature, low quenching distance, and high flame speed. The engine's exergy efficiency was the highest with hydrogen (34.23%), and it was about 24.23% and 24.08% with CNG and HCNG, respectively, at a high load (20.25 kW). This indicates a higher potential of hydrogen to convert the chemical energy input of fuel into heat and then power output. The exergy destruction was observed at minimum with hydrogen at all loads, and it was drastically reduced at high loads.

The combustion irreversibility calculated using species present during combustion was the main contributor to exergy destruction, and it decreased with hydrogen. The minimum combustion irreversibility was 11.75% with hydrogen, followed by HCNG and CNG with 16.46% and 18.88%, respectively, at high load. The high quality of heat due to high in-cylinder temperature and low entropy generation during combustion caused by fewer chemical species in hydrogen combustion are the main reasons for lower combustion irreversibility with hydrogen.

Sahoo and *Srivastava* [12] did a comparative energy and exergy analysis using a bi-fuel Compressed Natural Gas (CNG) spark ignition engine. The experiments were conducted for gasoline and CNG fuel at 1700 rpm and different operating loads from 5 to 30 Nm. The experiments were performed under stoichiometric air-fuel ratio and maximum brake torque ignition timing. Quantitative and qualitative analyses were conducted using the first and second law of thermodynamics, respectively. The effect of engine operating load on various energy and exergy parameters was compared for both fuels. Output energy concerning engine load was found higher for CNG compared to gasoline. Engine wall heat transfer was also higher in the CNG engine case due to its high combustion chamber temperature and lower burning velocity. The difference in heat transfer energy fraction between gasoline and CNG gradually increased with engine load. The exhaust energy was found to be maximum in the case of CNG under low operating load and reduced to a minimum at higher engine operating load. The unaccounted energy fraction was found lower for the CNG engine and reduced engine load. CNG exhibits the highest exergy efficiency (26.80%) compared to gasoline (25.50%) at a 30 Nm load. On average, a 2% higher exergy efficiency was observed with the CNG engine at all operating load conditions. This indicates CNG has a higher potential to convert chemical energy present in the fuel into useful work output. CNG shows lower exergy destruction at all operating loads than gasoline, reducing significantly at higher engine loads. In all operating loads, exergy transfer due to exhaust gas and heat transfer to the wall was higher in the case of CNG.

In a study by *Liu et al.* [13], the change rules and influence mechanism of injection pressure and timing on exergy terms at different working conditions are investigated based on a turbocharged diesel engine test platform, a multidimensional simulation model, and subsequent theoretical calculation. The detailed mechanism and distribution characteristic of exergy destruction was also studied at different injection parameters from the in-cylinder microscopic field to have a comprehensive analysis. The results show that exhaust exergy and exergy destruction are negatively correlated with injection pressure, but the influence of injection pressure on heat transfer exergy and exergy destruction is relatively weak. Secondly, advancing injection timing from 1.7°CA BTDC to 6.7°CA BTDC, the exergy efficiency and heat transfer exergy increase significantly, while the exhaust exergy and exergy destruction decrease gradually, compared with injection pressure, injection timing has a greater impact on exergy terms. Third, variation of exergy terms occurs mainly in the combustion process at different injection parameters. Fourth, the higher exergy destruction mainly concentrates in the region with an equivalence ratio of 1–1.5 at different injection pressures, and the EDR (exergy destruction rate) is proportional to HRR (heat release rate) in the same temperature range at different injection timing, the root influence causes of injection pressure and timing on exergy destruction are inhomogeneity of equivalent ratio and local temperature during the combustion process, respectively. Finally, increasing exergy efficiency is accompanied by a decrease in exergy destruction, and reasonable adjustment of injection parameters of the turbocharged diesel engine to enhance high-temperature and lean combustion characteristics during the combustion process of the in-cylinder mixture can effectively promote the exergy efficiency and restrain exergy destruction.

The study by *Bhatti et al.* [14] deals with energy and exergy analysis of variable compression ratio four-stroke spark-ignition engine based on experimental work. The effect of varying compression ratios from 6 to 10 is analyzed on both energy and exergy-based approaches. Both energy and exergy distributions are evaluated at different compression ratios for different rpm. The results show that as the compression ratio increased from 6 to 10, the maximum power output is obtained at a compression ratio 10 at 1800 rpm, i.e., 3.80 kW. The maximum energy and exergy efficiencies are found to be 28.55% and 27.35% respectively at a compression ratio of 9 for 1200 rpm. Entropy generation was found to be maximum for compression ratio 7 i.e. 36.47 W/K at 1800 rpm and

minimum for compression ratio 9 i.e. 15.68 W/K at 1200 rpm. The results of this work revealed that exergy destruction of 10.87 kW was found to be maximum at compression ratio 7 for 1800 rpm. This conclusion is drawn from the study that applying both energy and exergy analysis gives a more valuable understanding of the performance and improvement of internal combustion engines by locating and then reducing the exergy loss at that location. Application of alternative gaseous fuels, exhaust heat recovery techniques, and lean and low-temperature combustion strategies reduce these exergy losses.

In a study by *Rufino et al.* [15], exergetic analysis evaluates the exergetic balance on experimental data. When applied to an internal combustion engine, exergetic analysis can identify sources of inefficiency and potentialities for utilizing exergy rejected. To perform this analysis, experimental data were acquired for different operating conditions of a spark-ignition engine by using gasohol and hydrous ethanol as fuels. With these data, an exergetic analysis was carried out by evaluating the effects of engine operating parameters on associated irreversibilities. Afterward, a comparison between the exergetic analyses of hydrous ethanol and gasohol was presented. Finally, first and second law efficiencies were evaluated as engine speed, engine load, and air-fuel ratio functions. Exergy distributions of hydrous ethanol at different conditions and the accounts of exergy losses during engine operations were also evaluated.

In an investigation by *Jafarmadar* [16], the energy and exergy analyses are carried out in pre and main chambers of a Lister 8.1 Indirect Diesel Injection (IDI), engine diesel engine for two loads (BMEP of 2.96 bar and 5.9 bar as 50% and full load operations) at maximum torque engine speed (730 rpm). The energy analyses are carried out during a closed engine cycle using a Computational Fluid Dynamics (CFD) code. The pressure in the cylinder for two loads is compared with the corresponding experimental data and shows good agreement. Also, for the exergy analysis in the chambers, a developed in-house computational code is applied. Various exergy components are identified and calculated separately with the crank position at both loads. The results show that 56% and 77% of total irreversibility at partial and full load operations are related to the combustion process in the main chamber, respectively. This work demonstrates that multidimensional modeling can be used in complex chamber geometry to gain more insight into the effect of the flow field on the combustion process accounting for the second law of thermodynamics.

Numerous researchers have devised various strategies to improve the combustion efficiency of the internal combustion engine. Despite continuous improvement during the past decades, there is still scope for further development in engine performance. This paper by *Shinde et al.* [17] analyze the energy and exergy distribution of a single-cylinder 199.5 cc electronic fuel injected three-spark ignited high-speed petrol engine. The engine is operated at 25%, 50%, 75%, and 100% throttle positions for different speeds of 4000–10,000 rpm with an increment of 2000 rpm. From the detailed heat balance analysis, the best results obtained are maximum brake thermal efficiency of 34.9% corresponding to 6000 rpm at 50% throttle opening, minimum heat carried away by exhaust gas of 18.5% at 4000 rpm and 25% throttle position, minimum heat carried by cooling water as 13% for 10,000 rpm and 25% throttle, and the minimum unaccounted energy loss of 26.6% under the condition 8000 rpm and 75% throttle position. However, the best results of exergy analysis are second law efficiency of 51.93% corresponding to 4000 rpm and 25% throttle, maximum exergy transfer for useful work as 33.7% concerning 6000 rpm and 50% throttle, minimum exergy transfer for exhaust gas as 15.7% for 6000 rpm and 25% throttle, minimum exergy transfer associated with coolant of 4.6% at 4000 rpm and 25% throttle, and minimum exergy destruction of 39.4% corresponding to 8000 rpm and 50% throttle, respectively.

A study by *Odibi et al.* [18] uses the first and second laws of thermodynamics to investigate the effect of oxygenated fuels on the quality and quantity of energy in a turbocharged, common-rail six-cylinder diesel engine. This work was performed using a range of fuel oxygen content based on diesel, waste cooking biodiesel, and triacetin. The experimental engine performance and emission data were collected at 12 engine operating modes. Energy and exergy parameters were calculated, and results showed that the use of oxygenated fuels could improve thermal efficiency leading to lower exhaust energy loss. Waste cooking biodiesel (B100) exhibited the lowest exhaust loss fraction and highest thermal efficiency (6% higher than diesel). Considering the exergy analysis, lower exhaust temperatures obtained with oxygenated fuels resulted in lower

exhaust exergy loss (down to 80%) and higher exergetic efficiency (up to 10%). Since the investigated fuels were oxygenated, this study used the Oxygen Ratio (OR) instead of the equivalence ratio to better understand the concept. The OR has increased with decreasing engine load and increasing engine speed. Increasing the OR decreased the fuel exergy, exhaust exergy, and destruction efficiency. With the use of B100, there was very high exergy destruction (up to 55%), which was seen to decrease with the addition of triacetin (down to 29%).

A study by *Menzel et al.* [19] aims to apply multi-objective optimization to find conditions for opening and closing valves of maximum volumetric and thermal efficiency, evaluating through performance metrics two optimization methods. The inlet and exhaust valve timing were chosen as design variables. The multi-objective optimization methods used are Non-dominated Sorting Genetic Algorithm – II and Multi-Objective Differential Evolution. Simulations are performed for four different engine speeds. The compressible duct flow is numerically solved by the two-step Lax-Wendroff method with Total Variation Diminishing flow control. The performance metrics used in this study are maximum values, number of non-dominated solutions, spacing, hyper-volume, and time simulation. The results showed a Pareto front maximizing the volumetric efficiency and decreasing thermal efficiency and vice versa. The Multi-Objective Differential Evolution presented greater values than Non-dominated Sorting Genetic Algorithm – II, more non-dominated solutions, higher hyper-volume values, with the advantage of spending less computational time. Both approaches were able to optimize internal combustion engine efficiencies by finding the optimal valve timing sets. Moreover, it allows finding conditions for opening and closing valves that favor both efficiencies.

Exergy is a quantity of the work potential of energy from a given thermodynamic condition. Unlike energy, exergy can be destroyed, and for gasoline engines, the major source of this destruction is combustion. Therefore, to assess the quality of gasoline engines, *Kiani et al.* [20] examined the effect of inlet temperature and sparked timing on chemical, thermo-mechanical and total exergy of fuel using E0, E20, E40, E60, and E85 fuels. Results showed that by advancing the spark timing (20° bTDC), thermo-mechanical exergy has increased, but chemical exergy and total exergy have decreased. In addition, advance or delay in spark timing did not affect the fuel chemical exergy for the compression and expansion strokes. The effect of temperature on exergy parameters indicated that exergy parameters increased by reducing inlet temperature (320 K). In other words, the fuel chemical exergy at 320 K for E0, E20, E40, E60 and E85 fuels, increased by 7%, 7.1%, 7.2%, 7.2%, 7.3%, respectively, than 350 K and increased by 14%, 14.3%, 14.4%, 14.4% and 14.5% than 380 K.

In a study by *Boodaghi et al.* [21], the initial efforts concentrated on combining relationships of input and output parameters of hydrogen compressed natural gas spark-ignition engine. The quadratic regression models were conducted for all six responses: torque, carbon monoxide, brake-specific fuel consumption, methane, nitrogen oxides, and total hydrocarbon through response surface methodology and tested for adequacy by analysis of variance. The multi-objective desirability approach is employed for the optimization of input variables, namely, the hydrogen compressed natural gas ratio, excess air ratio (λ), and ignition timing (θi). Also, two factors, that is, manifold absolute pressure and engine speed, were fixed at 105 kPa and 1600 r/min, respectively. Results indicate that the optimal independent input factors are equal to λ of 1.178, hydrogen compressed natural gas ratio of 25.98%, and θi of 18 °CA before top dead center. Also, the optimal combination of responses is as follows: brake-specific fuel consumption of 219.334 g/kWh, the torque of 395 Nm, 30.189 g/kWh for nitrogen oxides, carbon monoxide equal to 5.093 g/kWh, total hydrocarbon of 0.633 g/kWh, and 0.572 g/kWh for methane. This study provided the significance of response surface methodology as an attractive technique for investigators for modeling. In this regard, the response surface methodology modeling and multi-objective desirability approach can be utilized to predict the emission and performance characteristics of the hydrogen compressed natural gas engines minutely.

The literature review shows that several researchers studied the internal combustion chamber's fuel performance in terms of energy, irreversibility, second law, and other mechanical parameters. However, Exergy analysis in a comparative view was implemented on the internal combustion engine in recent years. This method can determine several valuable exergy rates, irreversibility, exergy destruction, and efficiency. As it was mentioned, the importance of this method is due to the fact that

the energy performance alone is not a very good index to compare two engine performances when there are several fuel options. Furthermore, the fuel composition and performance of an engine are important factors in both in technical and policymaking scales. According to this fact, a similar study like those mentioned in the literature review seems necessary to be done in the Iranian car industry to have a better insight into the fuel policies and technologies. The mentioned gap in the literature suggested that the authors of this paper implement the exergy analysis in a comparative view for different conventional Iran-based fuels and analyze them in terms of second law performance. Also, the amount and source of exergy destruction or degradability of the workability can be determined by the exergy balance derived from the second law for thermal systems. In this research, a thermodynamic method for estimating the performance of a spark-ignition engine is proposed. Then the necessary definitions for the exergy analysis of the system are stated, and exergic comparisons are performed for different fuels. The use of quasi-dimensional modeling allows a more accurate analysis of the details of exergy transfer by effective factors than the conventional zero-dimensional method.

THEORETICAL SECTION

Thermodynamic modeling

The purpose of this section is to model the power generation process, including the compression, combustion, and expansion, in a four-stroke internal combustion engine by the quasi-dimensional method. Thus, using the equations of mass survival, the first law of thermodynamics, equilibrium reaction relations, quasi-complete gas governing relations and applied to each engine process, the macroscopic properties of the mixture inside the cylinder, such as pressure and temperature, And other quantities are calculated in different degrees of lameness, assuming the occurrence of thermodynamic processes in a quasi-equilibrium manner[21-30]. It is worth mentioning that the thermodynamic properties of the mixture inside the cylinder are determined at any given moment according to the composition of the ideal gases and based on the prevailing combustion reaction. In this research, the necessary thermodynamic relationships for each process have been developed molecularly. How to obtain mass equations is given in reference [9]. In modeling the engine power generation cycle processes, each crank angle is used as a computational step to discretize the developed equations. Thus, the thermodynamic properties in each step can be calculated by the iterative solution method provided by the relations and having the properties of the previous step. The description of the solution method is mentioned in references [31-42]. To simplify first law calculations, the following assumptions are made 1) The engine operates at a steady-state; 2) The entire engine, including the dynamometer, is selected as a control volume; 3) The combustion air and exhaust gas each form an ideal gas mixture; 4) Potential and kinetic energy effects of the combustion air, fuel stream, and exhaust gas are not considered.

Also, Table 1 below shows the composition of the studied fuels according to the ASTM standard tests.

Principles of modeling

The basic relationship used in the modeling process is the energy conservation relationship (1). In this regard, kinetic energy and operating fluid potential are neglected [11].

$$dU = \delta Q - \delta W + \sum h_i dn_i \quad (1)$$

In equation (1), the first expressions on the right indicate the heat transfer of the fluid inside the cylinder with the walls, and if the heat is absorbed from the wall, its value is positive[12]. The amount of heat transfer can be calculated by considering the effect of heat transfer, displacement from the Woschni equation, and radiation from the Annand equation according to Eq.n (2) [13-15]. The experimental coefficient concerning heat transfer is used to estimate better the engine's performance, determined for each fuel according to the experimental results [7, 16, 17]. The second expression refers to the exchange of the system with the environment and is calculated from the PV relationship. A positive value for this expression is obtained from the transfer of work from the fluid to the piston. The last expression is related to the transfer of energy in the system by the flow of the incoming or outgoing fluid, and for this expression, the fluid inflow is considered with a positive sign[43-56].

$$\dot{Q} = (C h_c (T_w - T) + \frac{4.3}{10^9}(T^4{}_w - T^4))A \quad (2)$$

Table 1: Fuel Composition of the studied fuels in this paper.

Parameter	Standard ID	Methane	Gasoline	Hydrogen
CO_2 content	ASTM D1945	53.12kg/1000ft^3	8.89kg/gallon	0
Net calorific value	ASTM D3588	53,000 kJ/kg	43,600 kJ/kg	120,000 kJ/kg
Gross calorific value	ASTM D3588	55,000 kJ/kg	47,000 kJ/kg	140,000 kJ/kg
Density	ASTM D3588	0.716kg/m^3	754 kg/m^3	0.090kg/m^3
Specific gravity	ASTM D3588	0.870	0.770	0.070
Molecular mass	ASTM D3588	16.04 g/mol	100.5 g/mol	2.02 g/mol
Flame Temperature	ASTM D3588	2210K	1299K	2400K

In Equation (2), T is the mixture temperature, T_w is the wall temperature, A is the heat transfer surface, h_c is the mixture's heat transfer coefficient, and C is the experimental coefficient[20].

Expansion and density

To calculate the macroscopic properties of the fluid during the compaction and expansion process, the first law of thermodynamics is applied to each crank angle, assuming there is no inlet and outlet fluid flow and exposure to the closed system[57-67]. Thus, to calculate the temperature and pressure at each crank angle, Equations (3) and (4) are obtained, respectively.

$$\frac{dT}{d\theta}=\frac{1}{nc_v}\left(\frac{dQ}{d\theta}-P\frac{dV}{d\theta}-\bar{u}\frac{dn}{d\theta}\right) \quad (3)$$

$$\frac{dP}{d\theta}=\frac{1}{V}\left(nR\frac{dT}{d\theta}+T\bar{R}\frac{dn}{d\theta}-P\frac{dV}{d\theta}\right) \quad (4)$$

In these relations, P is the mixture pressure, V is the volume, θ is the crank angle, n is the number of mol of the mixture, R is the universal constant of gases, and c_v is the specific heat capacity a constant volume. In Eq. (4), the expression for the compression process can be neglected, and $dn/d\theta$ the expansion, of the process, can be calculated by considering equilibrium reactions.[68]

Combustion

The system consists of two burned and unburned areas at the end of each computational step for the combustion process. These two areas have different temperatures and the same pressure [69]. By extending the first rule for this stage, the temperature of the unburned area, the temperature of the burned area, and the pressure of the chamber can be calculated from Equations (5), (6), and (7), respectively.

$$\frac{dT_u}{d\theta}=\frac{1}{n_u\bar{c}_{p,u}}\left(V_u\frac{dP}{d\theta}+P\frac{dQ_u}{d\theta}\right) \quad (5)$$

$$\frac{dT_b}{d\theta}=\frac{P}{n_b\bar{R}}\left(\frac{dV}{d\theta}-\frac{V_u}{n_u}\frac{dn_u}{d\theta}-\frac{V_b}{n_b}\frac{dn_b}{d\theta}-\frac{\bar{R}}{P\bar{c}_{p,u}}(V_u\frac{dP}{d\theta}+\frac{dQ_u}{d\theta})+\frac{V}{P}\frac{dP}{d\theta}\right) \quad (6)$$

$$\frac{dP}{d\theta}=\left(\frac{(\bar{c}_{v,u}-\bar{c}_{v,b})}{\bar{c}_{p,u}}V_u+\frac{\bar{c}_{v,b}}{\bar{R}}V\right)^{-1}-\left(1+\frac{c_{v,b}}{\bar{R}}\right)P\frac{dV}{d\theta}+\frac{dQ}{d\theta}+c_{v,b}\left(T_u\frac{dn_u}{d\theta}+T_b\frac{dn_b}{d\theta}\right)+(\bar{u}_u-\bar{u}_b)\frac{dn_b}{d\theta} \quad (7)$$

In these relationships, the subtitle u means unburned mixture and b means burnt mixture. It is important to note that some unburned mixture ignites and enters the burned area at each computational step[9]. Therefore, there is a fluid flow between the burned and scorched areas. The manifestation of this is the existence of ($dn_b/d\theta$, $dn_u/d\theta$) equations (6) and (7). According to the law of conservation of mass, these two expressions are related according to the equation $dn_b = -M_u / M_b dn_u$ in which M is the molar mass. To calculate $dn_u / d\theta$ equation (8) is used based on the existence of turbulent flame velocity [70].

$$\frac{dn_u}{d\theta}=-\bar{\rho}u_tA_f\left(\frac{dt}{d\theta}\right) \quad (8)$$

In Equation (8), ρ is the molar density, u_t is the turbulent velocity of the flame, A_f is the frontal surface of the flame, and t is the time.

The equation of turbulent flame velocity is often modeled based on the existing experimental relationships for slow flame velocity and considering the fold of the flame surface as the only effect of turbulence [9, 10]. The effect of turbulence is such that by increasing its amount, the combustion length remains constant in terms of the crankshaft [11,12, 17]. Some researchers have hypothesized that the velocity of a turbulent flame is proportional to its slow flame velocity and that its proportionality constant is a function of the intensity of the turbulence. *Hiroyasu* and *Kadota* considered the turbulence intensity proportional to the engine speed and presented Eq. (9) [71-80].

$$u_t = (1 + bN)u_l \tag{9}$$

In Equation (9), N is the engine speed of rounds per minute, and u_l is the slow flame speed. Also, b is the coefficient of proportionality of turbulence intensity with distance and is determined based on experimental results [10].

Slow flame velocity

The slow flame velocity is the physical and chemical property of the ready-to-ignite mixture and is the velocity by which the smooth, flat flame forehead advances in the ready-to-ignite mixture in a direction perpendicular to the plane [12, 16]. This study calculates the slow flame velocities for gasoline, methane, and hydrogen by the equations described below.

Hydrogen

Liu and *McFarlane* measured the slow flame velocity of a mixture of hydrogen, air, and water vapor using a laser doppler anemometer and photographing a conical flame using the Schellin imaging method. Their measurements led to the extraction of Eq. (10) for the slow flame ignition speed of the mentioned mixture [81-93].

$$u_l = a_1 + a_2(0.42 - X_{H2}) + a_3(0.42 - X_{H2})^7 \exp(a_6 X_{H2O}) T_u^{\,a_4 + a_5(0.42 - X_{H2})} \tag{10}$$

In Eq. (10), T_u is the temperature of the unburned mixture in Kelvin, X_{H2} molar ratio of hydrogen in the unburned mixture, and X_{H2O} molar ratio of water vapor. Also, coefficients a1 to a6 are presented in Table 2.

Methane

The calculation of the slow flame velocity of the methane-air mixture is based on the relationship proposed by Ref. [13]. The relationship presented by him is inspired by the results of the work of the pioneers in this field. He obtained Eq. (11) by collecting the effective parameters mentioned by other researchers. He validated his relationship by experimental results with less than 10% relative error under various combustion conditions.

$$u_t = u_{l,0}\left(\frac{T_u}{T_0}\right)^{\alpha}\left(\frac{P}{P_0}\right)^{\beta} \tag{11}$$

$$\alpha = \alpha_0 + \alpha_1\varphi + \alpha_2\varphi^4 + \alpha_3\left(\frac{T_u}{T_0}\right)^2\varphi^2$$

$$\beta = \beta_0 + \beta_1\varphi + \beta_2\varphi^4 + \beta_3\left(\frac{P}{T_0}\right)\left(\frac{T_u}{T_0}\right)^2\varphi^2$$

$$u_{l,0} = c_0\varphi^{c_1}\exp\left(c_2(\varphi + c_3)^2\right)$$

In Equation (11), φ is the equivalence ratio, and βi, αi, and ci are the coefficients of the equation, and their values are presented in Table 3. Also, for this relationship, the values related to reference temperature and pressure are T_0 = 300K and P_0 = 1 bar, respectively [11, 12].

Gasoline

The slow flame velocity of the gasoline-air mixture can be calculated from the interaction ratio of coke [1], Equation (12).

$$u_t = u_{l,0}\left(\frac{T_u}{T_0}\right)^{\alpha}\left(\frac{P}{P_0}\right)^{\beta} \tag{12}$$

$$\alpha = 2.18 - 0.8(\varphi - 1)$$

$$\beta = -0.16 + 0.22(\varphi - 1)$$

$$u_{l,0} = B_m + B_\varphi(\varphi - \varphi_m)^2$$

In Equation (12), the reference temperature and pressure T0 = 298 K and P0 = 1 atm. Also, the values of B_m, ϕ_m, and B_ϕ are 0.305 m/s, 1.21, and 0.459 m/s, respectively.

Exergy analysis

The exergy content of a substance indicates the extent to which it can do useful work. This exergy content increases as the system distance itself from the environment. The efficiency (exergy) of the system, in a certain state,

Table 2: Coefficients of equation u_l in equation (10) in meters per second [21].

Coefficient	$0.42 \leq X_{H2}$	$0.42 > X_{H2}$
a1	4.644×10^{-4}	4.644×10^{-4}
a2	-2.119×10^{-3}	9.898×10^{-4}
a3	2.344×10^{-3}	-1.264×10^{-3}
a4	1.57	1.57
a5	0.384	-0.248
a6	-2.21	-2.24

Table 3: The coefficients of the equation u_l in equation (11) in meters per second [13]

c0	1.508168	β_0	-0.5406	α_0	3.2466
c1	4.5386	β_1	0.1347	α_1	-1.0709
c2	-2.4481	β_2	-0.0125	α_2	0.1517
c3	-0.2248	β_3	2.2891×10^{-4}	α_3	-1.0359

as the most work that can be produced through the interaction of the system with its surroundings, while only the heat transfer of the system with the environment, to achieve thermal equilibrium, mechanical equilibrium, and chemical equilibrium Defined. The state in which the system reaches equilibrium with the environment is called the dead state [9, 10]. The existence of a mechanical and thermal balance between the system and the environment is called thermomechanical balance. If there is only a thermomechanical balance between the system and its surroundings, it is said to be in a dead state. The dead state is usually limited to one in which the chemical composition of the system is the same as the chemical composition of the system in the first case. The terms heat exergy and mechanical exergy are collectively called thermomechanical exergy[11]. Chemical exergy is defined as the ability to operate the system due to the occurrence of a reversible chemical reaction between system components and environmental components or due to the reversible passage of system components to ambient conditions and mixing with the environment until it reaches the dead state. It is studied thermomechanically [8, 12, 14]. Thermal equilibrium is achieved when the system's temperature equals its surroundings and mechanical equilibrium is achieved when there is no pressure difference between the system and its surroundings [5]. Chemical equilibrium is achieved only when the system does not contain any components that can produce work by interacting with its environment. The only system components that cannot react chemically with the atmosphere and form dead components are the environment components [15, 18]. The choice of reference environmental conditions greatly affects the system's efficiency because this reference determines the balance between the system and the environment. For temperature and pressure, environmental conditions are usually considered T_0 = 298.15 K and P_0 = 101325Pa, which can be changed depending on the system's operating conditions. The chemical composition of the environment is considered a mixture of oxygen, nitrogen, carbon dioxide, and water vapor with a mixture of ideal gases. The volume percentage of each component in the air mixture is decided based on the relative humidity of the air due to the presence of water vapor. In this research, the study is based on the relative humidity of 60%. In this case, the molar composition of the environment is 20.55% oxygen, 76.62% nitrogen, 0.03% carbon dioxide, 1.88% water vapor, and 0.92% other components. The molar ratio values of each component in different relative humidity can be obtained from the reference [15, 16-30].

According to the definitions made and the elimination of system heat transfer to the environment between the relations of the first law and the second law of thermodynamics, the exergy balance relation can be defined for a system according to Eq. (13). When encountering a closed system, the expressions related to the input and output of mass flow are removed from the equation[31-35].

$$\frac{dA_{sys}}{dt} = -\dot{E}x_Q + \dot{E}x_W + \dot{E}x_{f,out} - \dot{E}x_{f,in} - \dot{I} = 0 \qquad (13)$$

In Eq. (13), the first expression refers to the rate of exergy change within the system. The second expression refers to the rate of exergy transmitted by heat transfer, calculated from Eq. (14). In this regard, Q_j is the heat transfer from the system to the environment, and T_j is the temperature of the heat transfer boundary. In the exergy analysis of internal combustion engines, the instantaneous temperature inside the chamber is usually used as the system boundary temperature [8, 19].

$$\dot{E}x_Q = \int_j \left(1 - \frac{T_0}{T_j}\right)\dot{Q}_j \tag{14}$$

The third expression in Equation (13) is the rate of transfer of exergy associated with work, calculated from Eq. (15). In this regard, the second expression to the right of the equation represents the work done by the environment on the system and is not accessible to the system and must be deducted from the total work to achieve the exergy transmitted by the work [36-42].

$$\dot{E}x_w = \dot{W}_{sys} - P_0 \frac{dV_{sys}}{dt} \tag{15}$$

The fourth and fifth expressions in Equation (13) are the exergy rate of the current entering and leaving the system, respectively, obtained from Equation (16).

$$\dot{E}x_f = \sum_i \dot{n}_k \bar{b}_k \tag{16}$$

In Eq. (16), b is the molar exergy of mass flow and consists of thermomechanical and chemical exergy according to Eq. (17).

$$\bar{b} = \sum_i y_i \left(\bar{b}_i^{tm} + \bar{b}_i^{ch}\right) \tag{17}$$

The current thermomechanical exergy of component i is obtained from the difference between the present conditions and the environmental conditions according to Eq. (18).

$$\bar{b}_i^{tm} = \bar{h}_i - \bar{h}_{i,0} - T_0\left(\bar{s}_i - \bar{s}_{i,0}\right) \tag{18}$$

The chemical exergy of component i is calculated in terms of presence or absence in the environment according to Eqs (19) and (20), respectively. Each the non-existent component in the environment is considered a potential fuel.

$$\bar{b}_i^{ch} = \bar{R}\,T_0 \ln \frac{y_i}{y_{i,00}} \tag{19}$$

In Eq. (19), y is the molar ratio in the mixture, and y_{00} is the molar ratio in the environmental conditions.

Eq. (20) is obtained concerning the combustion reaction of a non-existent component in the environment, the products of which are components of the environment, and the values of *v* are related to the stoichiometric coefficients of this reaction[43-50].

$$\bar{b}_{fuel,pure}^{ch} = -\Delta\bar{g}_{T_0}^{o} + \bar{R}\,T_0 \ln \frac{(y_{O2,00})^{v_{O2}}}{\prod_P (y_{i,00})^{v_i}} \tag{20}$$

$$\Delta\bar{g}_{T_0}^{o} = \sum_P v_i \bar{g}_{i,T_0}^{o} - v_{O2}\bar{g}_{O2,T_0}^{o} - \bar{g}_{fuel,T_0}^{o}$$

$$\bar{g}_i = \bar{h}_i - T\bar{s}_i$$

In Equation (20), h is the molar enthalpy, s is molar entropy, and g is the molar standard Gibbs free energy. The last expression in Eq. (13) indicates the rate of irreversibility and exergy destruction within the system during the process.

Determining the boundary of the system has a significant effect on the value obtained for this expression. Another way to calculate this expression is to use the entropy equilibrium relation within the system to calculate the entropy generation rate by which the irreversibility can be obtained from the relation $I = T_0 S_{gen}$. A detailed description of how to obtain equations (13) to (20) is given in references [5,8, 14, 51-54].

RESULTS AND DISCUSSION

In this part, the validation of the engine model code performed by this paper results is performed using the experimental results provided by Pourkhasalian and his colleagues [26] on the Mazda B2000i engine. Assumptions and data are listed in Table 4, and Mathlab 2016a is used to validate the pressure curve inside the cylinder in terms of crank angle. The validation results for hydrogen, gasoline, and methane fuels are given in Figs. 1, 2, and 3, respectively. As can be seen from these figures, the code can provide a good estimate of system performance. Of course, this result is due to the correct selection of the experimental coefficients in the engine simulation process, heat transfer coefficient, and turbulent velocity coefficient. These experimental coefficients are determined by comparing the code results with the experimental engine results. The reason for these experimental coefficients is the existing simplification assumptions, such as the assumption of spherical flame progression and not observing the effects of turbulence in this form of modeling.

Error analysis of the results obtained in Figs. 1, 2, and 3 show that the code developed by adjusting the experimental constants can trace the maximum pressure relative to the spark time with a relative error of 21%, 22%, and 10%. The order is for hydrogen, gasoline, and

Table 4: Engine specifications under test [16].

Parameter	
Engine type	Four-stroke ignition
Number of cylinders	4
Suction type	natural
Piston stroke	86(mm)
Cylinder diameter	86(mm)
length of the connecting rod	153(mm)
Density ratio	8.6
Spark plugs per cylinder	1
Inlet valve opening time	10 ° btdc
Inlet valve closing time	49 ° abdc
Exhaust valve opening time	55 ° bbdc
Exhaust valve closing time	12 ° atdc

methane. Also, the highest deviation of the pressure estimate from the experimental results for hydrogen and gasoline is 28% and 17% at the maximum pressure of the experimental results, and for methane is 25% at 450 °C. However, the average error values for this parameter are less than 5%, 6%, and 4%, respectively. Compared to the ignition rate of gasoline, the high error of hydrogen at one point is its high ignition rate, and the reason for the high error of methane at one point of its low ignition rate. These cases lead to non-compliance with the degree of ignition delay from Benson's assumption, which exacerbates the error at one point. Benson's assumption is based on considering the ignition delay as the amount of time required for combustion to be one-thousandth of the total volume of the combustion chamber [10].

A comparison of the simulation and the code results the brake power characteristic and the specific brake consumption of the engine are presented in Table 5. These results indicated a relative error of 0.8%, 4%, and 5% for hydrogen, gasoline, and methane, respectively, for brake power. And also a relative error of 12%, 10%, and 14% for hydrogen, and methane, respectively, for specific brake consumption of the engine. In this research, the relation presented by Hood is used to calculate the frictional force [93-110].

Next, the engine exergy is analyzed with the mentioned geometric characteristics and operating conditions listed in Table 6. According to Eq. (13), the methods of transferring

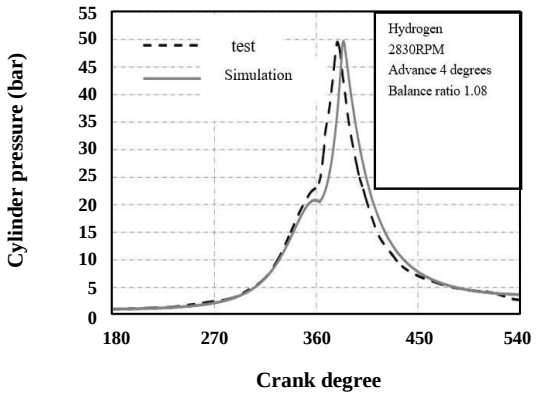

Fig. 1: Pressure change curve in terms of crank angle for hydrogen fuel.

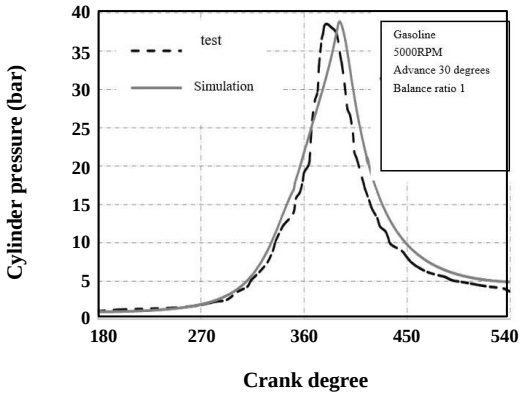

Fig. 2: Pressure change curve in terms of the crank angle for gasoline fuel.

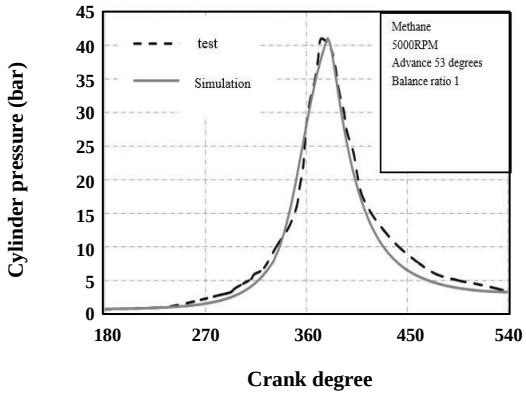

Fig. 3: Pressure change curve in terms of crank angle for methane fuel.

Table 5: Comparison of simulation results and experimental results for BSFC and BMEP performance characteristics.

Fuel	BMEP (bar)		BSFC (g/kWh)	
	Test	Simu.	Test	Simu.
Hydrogen	7.92	7.85	107	120
Gasoline	8.40	8.59	292	322
Methane	5.89	5.60	275	314

Table 6: Engine exergy analysis conditions.

Parameter	value
Balance ratio	1
Engine speed	3000(rpm)
Advance hydrogen spark	4° before the high point of death
Gasoline spark advance	18° before high death point
Methane spark advance	36° before high death point
Suction temperature	335(K)
Suction pressure	1(bar)
Wall temperature	435(K)

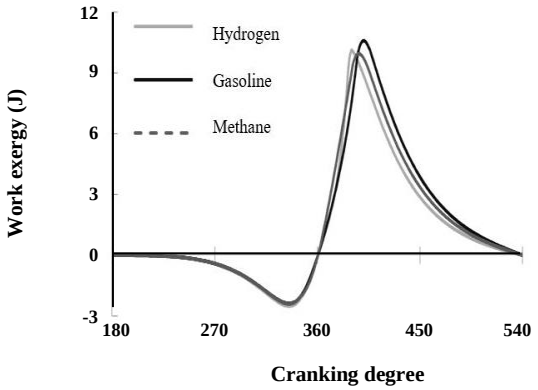

Fig. 4: Exergy changes transmitted by work according to the crank angle.

of transferring the input exergy to the heat transfer motor are work transfer and irreversibility in the face of a closed system. The effect of each factor is examined below [21, 22].

The amount of exergy transmitted by the work in terms of crankshaft for different fuels is shown in Fig. 4. As can be seen from this figure, the exergy transmitted by work to the point of high death is negative. The reason for this is the work done by the cylinder on the system. Another result of this figure is the higher maximum point of the gasoline curve, while gasoline has the lowest maximum pressure. The reason for this is the occurrence of maximum gasoline pressure at points far from the point of high death, which is accompanied by more volume change. Therefore, the change in pressure and volume determine the amount and location of maximum work exergy[111-119].

The amount of exergy transmitted by heat transfer in terms of crankshaft for different fuels is shown in Fig. 5. As shown from this figure, heat-transferred exergy is negative, except for the initial degrees of compaction. This indicates heat transfer out of the system due to the higher temperature of the system. Also, the maximum rate of thermal exergy transfer is related to the combustion process which the temperature and the amount of turbulence of the mixture inside the cylinder are higher. Other results of this figure can be:

Pointed to the higher maximum point of the hydrogen curve. This is due to the high flammability of hydrogen and its higher combustion temperature. This paves the way for more heat transfer to the end of the hydrogen cycle. This higher heat transfer causes a higher rate of temperature decrease in the hydrogen engine, and its heat transfer rate in the last stages of the cycle is closer to gasoline and methane. The amount of irreversibility produced in the closed cycle of the engine in terms of crankshaft for different fuels is shown in Fig. 6. In analyzing this figure, it should be noted that the start and end time the combustion process for each fuel varies according to the ignition timing and the flame propagation speed. As can be seen from this figure, the irreversibility rate in the stages of compaction and expansion is very small, almost zero, and only in the combustion stage is the existence of irreversibility evident. The reason for this is the type of heat transfer boundary temperature selected. Here, the instantaneous temperature of the operating fluid inside the cylinder is used for this purpose, and in the combustion stage, the temperature of the same area is considered the temperature of the heat transfer boundary. This choice, because it prevents the irreversibility of the heat transfer process between heat sources with a large temperature difference makes it possible to observe only the effect of the nature of the process and leads to a better analysis of irreversibility. If the combustion chamber wall

temperature is selected as the system boundary temperature, the irreversibility value will change between the operating fluid temperature and the combustion chamber wall. The existence of irreversibility in the combustion process is completely consistent with the existing physical understanding of this process, even assuming the equilibrium occurs as an irreversible process. A noteworthy point is the location of the maximum irreversibility. This point is exactly where the most combustible fuel is in the combustion process, and the highest temperature is created during the combustion (causing the highest exergy destruction due to the highest temperature difference). This indicates the effect of combustion rate on the rate of production irreversibility. In Fig. 6, the reason for the sudden increase in irreversibility at the beginning of the combustion phase is the use of the Benson hypothesis [12] in predicting ignition delay. In this assumption, some fuel is ignited during the compaction process, and the effect of the ignited fuel is seen in the first step of the combustion process calculations. Another noteworthy point is the higher maximum point of the gasoline curve due to the higher ignition rate of hydrogen. This indicates that the process of burning gasoline is more irreversible than hydrogen.

Changes in the amount of exergy of the mixture inside the cylinder, the total thermomechanical and chemical exergy, in the closed cycle of the engine in terms of crankshaft for different fuels are shown in Fig. 7. As shown from this figure, the input exergy to the system is maximal for the gasoline engine. Due to the same temperature and pressure of the inlet mixture for all fuels, more chemical exergy of the gasoline engine can be exalted. One of the reasons for this is the mass of more incoming gasoline than hydrogen pointed. The chemical exergy of methane is certainly minimal, according to Fig. 7, and the mass of methane input, close to gasoline. Other results of this figure include increased system exergy to TDC due to work and piston and decreased later stages.

A comparison of the integral values of different exergy transfer methods in terms of the percentage of input exergy for different fuels is presented in Fig. 8. This figure shows that the share of exergy transferred by work from the input exergy for all three fuels is approximately equal. Other results in Fig. 8 include a higher share of heat transfer for hydrogen, a lower share of irreversibility for

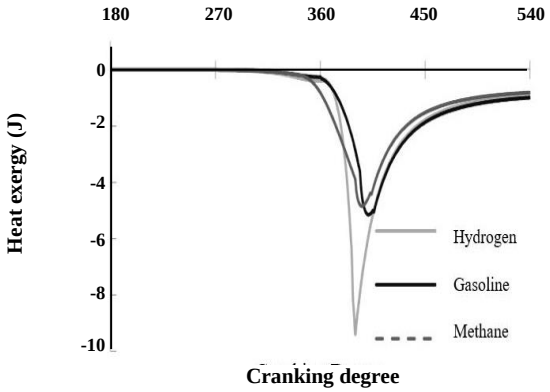

Fig. 5: Heat-transferred exergy changes in the crank angle.

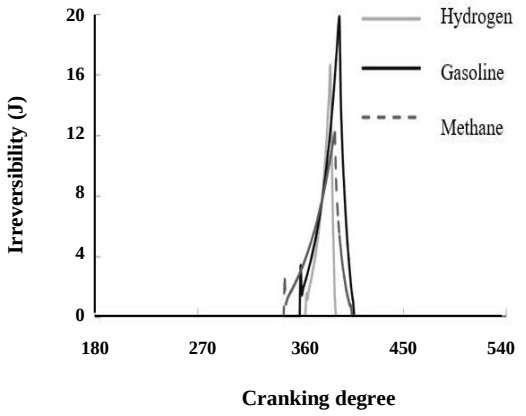

Fig. 6: Irreversible changes in the crank angle.

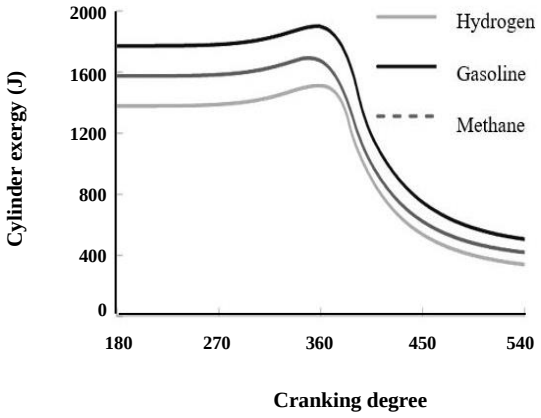

Fig. 7: Exergy changes of the system according to the crank angle.

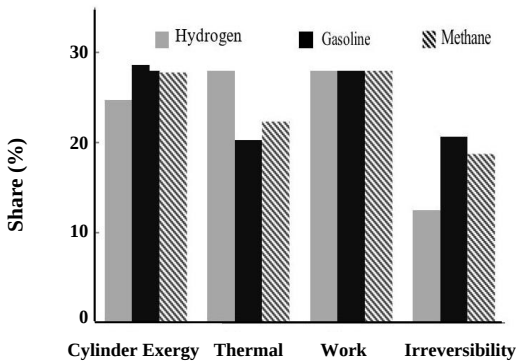

Fig. 8: Comparison of exergy transfer methods in terms of inlet exergy for different fuels at the end of the closed engine cycle.

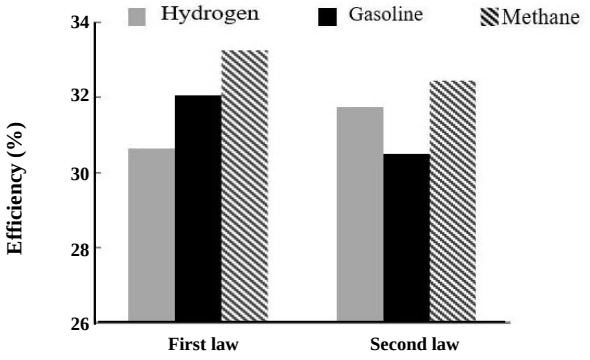

Fig. 9: Comparison of the efficiency values of the first and second laws for different fuels.

hydrogen, and an almost equal share of irreversibility for gasoline and methane. This indicates the least amount of input exergy degradation due to the irreversibility of hydrogen. Also, the highest percentage of exergy in the mixture at the end of the closed engine cycle is related to gasoline.

In the next step, the comparison of the indicator efficiency values of the first law and the second law of thermodynamics for different fuels is presented in Fig. 9. The basis for calculating the first law is the ratio of productive work to the calorific value of the input fuel [1] and the basis for calculating the second law is the ratio of productive work to the exergy of the input mixture to the engine ($\dot{W}/\dot{E}x_{f,in}$) [15]. From the results of Fig. 9, it is clear that the efficiency values of the first and second laws are close to each other. This result, considering the predominant contribution of the chemical exergy of the fuel to the exergy of the inlet mixture to the engine, is consistent with the experimental relation presented by *Brzustowski* and *Brena* [15] for the chemical exergy of the fuel, the amount of which is estimated.

At this stage, comparing the values of different types of exergy transmission at the end of the power cycle for different engine speeds has been studied. For this purpose, Figs. 10, 11, and 12 are presented for hydrogen, gasoline, and methane fuels.

The curves used in these figures provide a cumulative representation of the desired values; In this way, the value of each expression is obtained from the difference between its characteristic line and the previous line, and in each round, the highest point indicates the amount of exergy of the mixture entering the engine. As can be seen from these figures, the input mixture's exergy is equal for all cycles. The reason for this is to consider the same input conditions for different cycles in the simulation. Other results of these figures include a decrease in heat exergy with increasing distance due to reduced heat transfer time. Also, we can point to the almost irreversible rate for different periods. The reason for this is the same amount of inlet fuel, and the length of combustion in terms of crank angle is almost the same for different cycles, and as a result, the rate of fuel combustion is almost the same at the corresponding crank angles, taking into account the advance of different sparks. It is important to note that the combustion rate is higher at higher speeds, but due to the equilibrium reactions used in the combustion simulation, the amount of fuel burned at each crank angle affects irreversible production. Other results include an increase in the exergy transferred by the work and an increase in the mixture inside the cylinder due to the increase in speed.

At this stage, comparing the values of different types of exergy transmission at the end of the power cycle for different equivalence ratios has been studied. For this purpose, Figs. 13, 14, and 15 are presented for hydrogen, gasoline, and methane fuels. The curves used in these figures also provide a cumulative representation of the desired values. As can be seen from these figures, the amount of exergy in the inlet mixture increases with the increasing equivalence ratio, and the reason for this is the increase in the amount of fuel in the inlet mixture. Also,

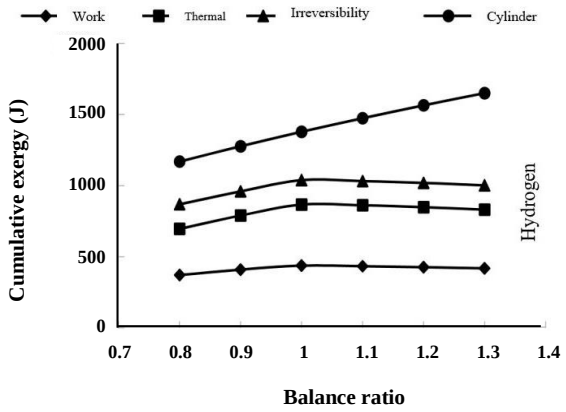

Fig. 13: The curve of changes in the values of the exergy balance relation at the end of the power cycle in terms of the equivalence ratio for hydrogen.

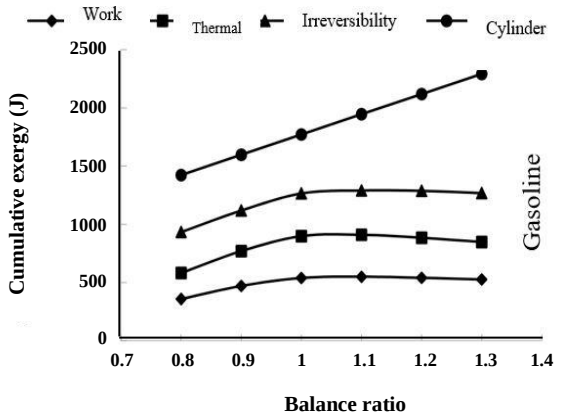

Fig. 14: The curve of changes in the values of the exergy balance relation at the end of the power cycle in terms of the balance ratio for gasoline.

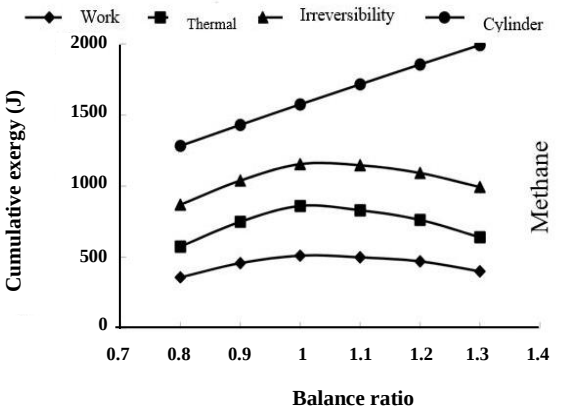

Fig. 15: The curve of changes in the values of the exergy balance relation at the end of the power cycle in terms of the equivalence ratio for methane.

we can mention the increase in the share of exergy of the outlet fluid by increasing the equivalence ratio, especially for the ratio of concentrated equilibria. The reason for this should be sought in the occurrence of incomplete combustion and the combination of exhaust gases for the ratio of equilibria greater than stoichiometric conditions. Under these conditions, the molar fraction of gases that do not exist under standard environmental conditions, carbon monoxide and hydrogen, increases between the exhaust gases. As mentioned in the explanations for the exergy analysis, these gases have chemical exergy. The concentrated equivalence ratio is associated with a large increase in the exergy of the exhaust gases so that they occupy a large share of the inlet exergy. Other results of these shapes include increasing the transferred exergy with work and heat to a certain equivalence ratio and then decreasing them. This equivalence ratio is 1.1 for gasoline and 1 for hydrogen and methane. This result follows the experimental observations [1] of the maximum engine output in the balance ratio close to 1. Other results include a decrease in the irreversible share of input exergy by increasing the equivalence ratio.

CONCLUSIONS

In this research, a mathematical model based on thermodynamic principles to predict the performance of spark-ignition internal combustion engines is presented. Also, the necessary conceptual bases for performing exergy analysis of the system have been established by defining the term exergy and creating the corresponding exergy balance equations and applying them to closed systems and control volumes. The results of the proposed model for hydrogen, gasoline, and methane fuels in comparison with the experimental results according to the mean error of 5, 6, and 7% for the in-cylinder pressure parameter, the relative error of 0.8, 4, and 5% for braking power, and relative error of 12, 10, and 14% are approved for brake consumption. The results of engine exergy analysis show that the combustion process is the dominant factor in entropy production in the closed cycle of the engine. The results of this study for the ratio of air to fuel stoichiometry can be given to the percentage of exergy transferred by working approximately equal to all three fuels, a higher percentage of exergy heat transfer for hydrogen, lower percentage of irreversibility for hydrogen, higher percentage of irreversibility for gasoline and

a higher percentage of exergy for gasoline at the end of the closed cycle of the engine pointed. Also, the exergy analysis results in different operating conditions show that increasing the engine speed increases the exergy transfer with work, decreases the exergy transfer with heat, and has almost no effect on irreversibility. On the other hand, increasing the balance ratio increases the inlet exergy to the engine, increases the share of the exergy mixture in the cylinder at the end of the power cycle, and decreases the irreversible share of inlet exergy.

Acknowledgments

The authors thank the scientific support of the Amirkabir University of Technology.

Nomenclature

A	Area, m^2
A_{sys}	System Performance, J
b	Mol current exergy, J / mol
cp	Specific heat capacity at constant pressure, J / mol.K
cv	Specific heat capacity is constant volume, J / mol.K
Ex	Exergy, J
G	Gibbs Molly standard free energy, J / mol
h	Enthalpy molar, J / mol
hc	Transfer heat transfer coefficient, W / m^2.K
I	Irreversibility, J
M	Molar mass, kg/mol
n	Number of moles, mol
P	Pressure, Pa
Q	Heat transfer, J
R	Universal gas constant, J / mol.K
s	Molly entropy, J / mol.K
Sgen	Entropy Generation, J / K
SA	Spark advance, º
T	Temperature, K
t	Time, s
U	Internal Energy, J
$\bar{u}$	Internal Molly Energy, J / mol
u	Ingitation velocity, m / s
V	Volume, 3m
W	Work, J
y	Molar ratio

Greek signs

Θ	Crank angle
φ	Balance ratio

subscript

b	Burnt mixture
f	Flame forehead
l	Laminar
t	Turbulent
u	Unburned mixture
w	Wall
0	Reference conditions

Superscript

ch	Chemical
tm	Thermomechanical

Received : Oct. 1, 2021 ; Accepted : Dec. 4, 2021

REFERENCES

[1] Ma B., Yao A., Yao C., Wu T., Wang B., Gao J., Chen C., Exergy Loss Analysis on Diesel Methanol Dual Fuel Engine under Different Operating Parameters, *Applied Energy*, **261**: 114483 (2020).

[2] Faizal M., Saidur R., Comparative Thermodynamic Analysis of Gasoline and Hydrogen Fuelled Internal Combustion Engines, *International Journal of Advanced Scientific Research and Management*, **2(3)**: 12-18 (2017).

[3] Verma S., Das L.M., Bhatti S.S., Kaushik S.C., A Comparative Exergetic Performance and Emission Analysis of Pilot Diesel Dual-Fuel Engine with Biogas, CNG and Hydrogen as Main Fuels, *Energy Conversion and Management*, **151**: 764-777 (2017).

[4] Feng H., Wang X., Zhang J., Study on the Effects of Intake Conditions on the Exergy Destruction of Low Temperature Combustion Engine for a Toluene Reference Fuel, *Energy Conversion and Management*, **188**: 241-249 (2019).

[5] Bejan A., "Advanced Engineering Thermodynamics", John Wiley & Sons Inc. (2016).

[6] Azoumah Y., Blin J., Daho T., Exergy Efficiency Applied for the Performance Optimization of a Direct Injection Compression Ignition (CI) Engine Using Biofuels, *Renewable Energy*, **34(6)**: 1494-1500 (2009).

[7] Nieminen J., Dincer I., Comparative Exergy Analyses of Gasoline and Hydrogen Fuelled ICEs, *International Journal of Hydrogen Energy*, **35(10)**: 5124-5132 (2010).

[8] Mahabadipour H., Srinivasan K.K., Krishnan S.R., An Exergy Analysis Methodology for Internal Combustion Engines Using a Multi-Zone Simulation of Dual Fuel Low Temperature Combustion, *Applied Energy*, **256**: 113952 (2019).

[9] Elfasakhany A., The Effects of Ethanol-Gasoline Blends on Performance and Exhaust Emission Characteristics of Spark Ignition Engines, *International Journal of Automotive Engineering*, **4**: 609-620 (2014).

[10] Doğan B., Erol D., Yaman H., Kodanli E., The Effect of Ethanol-Gasoline Blends on Performance and Exhaust Emissions of a Spark Ignition Engine Through Exergy Analysis, *Applied Thermal Engineering*, **120**: 433-443 (2017).

[11] Dhyani V., Subramanian K.A., Experimental Based Comparative Exergy Analysis of a Multi-Cylinder Spark Ignition Engine Fuelled with Different Gaseous (CNG, HCNG, And Hydrogen) Fuels, *International Journal of Hydrogen Energy*, **44(36)**: 20440-20451 (2019).

[12] Sahoo S., Srivastava D.K., Quantitative and Qualitative Analysis of Thermodynamic Process of a Bi-Fuel Compressed Natural Gas Spark Ignition Engine, *Environmental Progress & Sustainable Energy*, e13583 (2021).

[13] Liu C., Liu Z., Tian J., Han Y., Xu Y., Yang Z., Comprehensive Investigation of Injection Parameters Effect on a Turbocharged Diesel Engine Based on Detailed Exergy Analysis, *Applied Thermal Engineering*, **154**: 343-357 (2019).

[14] Bhatti S.S., Verma S., Tyagi S.K., Energy and Exergy Based Performance Evaluation of Variable Compression Ratio Spark Ignition Engine Based on Experimental Work, *Thermal Science and Engineering Progress*, **9**: 332-339 (2019).

[15] Rufino C.H., de Lima A.J., Mattos A.P., Allah F.U., Bernal J.L., Ferreira J.V., Gallo W.L., Exergetic Analysis of a Spark Ignition Engine Fuelled with Ethanol, *Energy Conversion and Management*, **192**: 20-29 (2019).

[16] Jafarmadar S., Three-Dimensional Modeling and Exergy Analysis in Combustion Chambers of an Indirect Injection Diesel Engine, *Fuel*, **107**: 439-447 (2013).

[17] Shinde B.J., Karunamurthy K., Ismail S., Thermodynamic Analysis of Gasoline-Fueled Electronic Fuel Injection Digital Three-Spark Ignition (EFI-DTSI) Engine, *Journal of Thermal Analysis and Calorimetry*, **141(6)**: 2355-2367 (2020).

[18] Odibi C., Babaie M., Zare A., Nabi M.N., Bodisco T.A., Brown R.J., Exergy Analysis of a Diesel Engine with Waste Cooking Biodiesel and Triacetin, *Energy Conversion and Management*, **198**: 111912 (2019).

[19] Menzel G., Och S.H., Mariani V.C., Moura L.M., Domingues E., Multi-Objective Optimization of the Volumetric and Thermal Efficiencies Applied to a Multi-Cylinder Internal Combustion Engine, *Energy Conversion and Management*, **216**: 112930 (2020).

[20] Kian M.K.D., Rostami S., Eslami M., Yusaf T., Sendilvelan S., The Effect of Inlet Temperature and Spark Timing on Thermo-Mechanical, Chemical and the Total Exergy of an SI Engine Using Bioethanol-Gasoline Blends, *Energy Conversion and Management*, **165**: 344-353 (2018).

[21] Boodaghi H., Etghani M.M., Sedighi K., Numerical Study of Hydrogen Addition on the Performance and Emission Characteristics of Compressed Natural Gas Spark-Ignition Engine Using Response Surface Methodology and Multi-Objective Desirability Approach, *International Journal of Engine Research*, **22(8)**: 2575-2596 (2021).

[22] Hoseinzadeh S., Garcia D A., Numerical Analysis of Thermal, Fluid, and Electrical Performance of a Photovoltaic Thermal Collector at New Micro-Channels Geometry, *Journal of Energy Resources Technology*, **144(6)**: 062105 (2021).

[23] Mahmoudan A., Samadof P., Hosseinzadeh S., Garcia D.A., A Multigeneration Cascade System Using Ground-source Energy with Cold Recovery: 3E Analyses and Multi-objective Optimization, *Energy*, 121185 (2021).

[24] Hoseinzadeh S., Stephan Heyns P., Advanced Energy, Exergy, and Environmental (3E) Analyses and Optimization of a Coal-Fired 400 MW Thermal Power Plant, *Journal of Energy Resources Technology*, **143(8)**: 082106 (2021).

[25] Naderi A., Qasemian A., Shojaeefard M.H., Samiezadeh S., Younesi M., Sohani A., Hoseinzadeh S., A Smart Load-Speed Sensitive Cooling Map to Have a High-Performance Thermal Management System in an Internal Combustion Engine, *Energy*, **229**: 120667 (2021).

[26] Pourkhesalian A.M., Shamekhi A.H., Salimi F., Alternative Fuel and Gasoline in an SI Engine: A Comparative Study of Performance and Emissions Characteristics, *Fuel*, **89(5)**: 1056-1063 (2010).

[27] Rani V.A., Prabhakaran D., Thirumarimurugan M., Modelling and Control of pH in a Continuous Stirred Tank Reactor (CSTR), *J. Environ. Prot. Ecol.*, **21(2)**: 413-422 (2020).

[28] Ma X., Kexin Z., Yonggang W., Ebadi A.G., Toughani M., Investigation of Low-Temperature Lipase Production and Enzymatic Properties of Aspergillus Niger, *Iran. J. Chem. Chem. Eng. (IJCCE)*, **40(4)**: 1364-1374 (2021).

[29] Liu W., Zhang H., Gong J., Liu J., Advanced Treatment of Dyed Wastewater from Papermaking with Wastepaper Based on the Fenton Method, *J. Environ. Prot. Ecol.*, **21(2)**: 433-442 (2020).

[30] Soleimani-Amiri S., Asadbeigi N., Badragheh S., A Theoretical Approach to New Triplet and Quintet (nitrenoethynyl) alkylmethylenes,(nitrenoethynyl) alkylsilylenes,(nitrenoethynyl) alkylgermylenes, *Iran. J. Chem. Chem. Eng. (IJCCE).*, **39(4)**: 39-52 (2020).

[31] Soceanu A., Dobrinas S., Popovici I.C., Jitariu D., Health Risk Assessment of Heavy Metals in Seafood. *J. Environ. Prot. Ecol.*, **21(2)**: 490-497 (2020).

[32] Ahmadi S., Hosseinian A., Delir Kheirollahi Nezhad P., Monfared A., Vessally E., Nano-Ceria (CeO2): An Efficient Catalyst for the Multi-Component Synthesis of a Variety of Key Medicinal Heterocyclic Compounds, *Iran. J. Chem. Chem. Eng. (IJCCE).*, **38(6)**: 1-19 (2019).

[33] Burlacu I.F., Favier L., Matei E., Predescu C., Deák G., Photocatalytic Degradation of a Refractory Water Pollutant Using Nanosized Catalysts. *J. Environ. Prot. Ecol.*, **21(2)**: 571-578 (2020).

[34] Vessally, E., Mohammadi, S., Abdoli, M., Hosseinian, A., Ojaghloo, P., Convenient and Robust Metal-Free Synthesis of Benzazole-2-Ones Through the Reaction of Aniline Derivatives and Sodium Cyanate in Aqueous Medium, *Iran. J. Chem. Chem. Eng. (IJCCE).*, **39(5)**: 11-19 (2020).

[35] Su D., Jing W., Intelligent Pid Driving and Control in the Centrifugal Microfluidic Chip Environment, *J. Environ. Prot. Ecol.*, **21(2)**: 644-653 (2020).

[36] Paduretu C.C., Apetroaei M.R., Apetroaei G.M., Atodiresei D., Rau I., Dyes Adsorption by Using Different Types of Chitosan for Decontamination of Cleaning Waters from Chemical Carriers, *J. Environ. Prot. Ecol.*, **21(1)**: 28-36 (2020).

[37] Jalali Sarvestani M.R., Charehjou P., Fullerene (C20) as a Potential Adsorbent and Sensor for the Removal and Detection of Picric Acid Contaminant: DFT Studies, *Central Asian Journal of Environmental Science and Technology Innovation*, **2(1)**: 12-19 (2021).

[38] Rekha K., Thenmozhi D.R., Characterisation and Utilisation of Sugarcane Bagasse Ash as Pozzolanic Material and Its Effect on Mechanical Strength of Concrete, *J. Environ. Prot. Ecol.*, **21(1)**: 268-279 (2020).

[39] Gharibzadeh F., Vessally E., Edjlali L., Es' haghi M., Mohammadi R., A DFT Study on Sumanene, Corannulene and Nanosheet as the Anodes in Li−Ion Batteries, *Iran. J. Chem. Chem. Eng. (IJCCE)*, **39**: 51-62 (2020).

[40] Cani X.H., Malollari I., Nuro A., Buzo R., Classification of Hydrocarbons Content in Used Tyres Pyrolytic Oil, by Gas Chromatography Method, *J. Environ. Prot. Ecol.*, **21(1)**: 300-307 (2020).

[41] Vessally E., Hosseinian A., A Computational Study on the Some Small Graphene-Like Nanostructures as the Anodes in Na−Ion Batteries, *Iran. J. Chem. Chem. Eng.(IJCCE)*, **40**: 691-703 (2021).

[42] Hornet M., Cirstolovean I.L., Nastac D.C., Todor R., Natural Ventilation for Amphitheatres-A Way of Increasing Indoor Air Quality by Decreasing Energy Consumption, *J. Environ. Prot. Ecol.*, **21(1)**: 10-18 (2020).

[43] Vessally E., Farajzadeh P., Najafi E., Possible Sensing Ability of Boron Nitride Nanosheet and its Al– and Si–Doped Derivatives for Methimazole drug by Computational Study, *Iran. J. Chem. Chem. Eng. (IJCCE)*, **40(4)**:1001-1011(2021).

[44] Ivanova L.P., Vassileva P.S., Gencheva G.G., Detcheva, A.K., Feasibility of Two Bulgarian Medicinal Plant Materials for Removal of Cu^{2+} Ions from Aqueous Solutions, *J. Environ. Prot. Ecol.*, **21(1)**: 37-45 (2020).

[45] Hashemzadeh B., Edjlali L., Delir Kheirollahi Nezhad P., Vessally E., A DFT Studies on a Potential Anode Compound for Li-Ion Batteries: Hexa-Cata-Hexabenzocoronene Nanographen, *Chem. Rev. Lett.*, (2021).

[46] Salehi N., Vessally E., Edjlali L., Alkorta I., Eshaghi M., Nan@Tetracyanoethylene (n=1-4) Systems: Sodium salt vs Sodium Electrode, *Chem. Rev. Lett.*, **3**: 207-217 (2020).

[47] Sreerama L., Vessally E., Behmagham F., Oxidative Lactamization of Amino Alcohols: An Overview, *J. Chem. Lett.*, **1**: 9-18 (2020).

[48] Majedi S., Sreerama L., Vessally E., Behmagham F., Metal-Free Regioselective Thiocyanation of (Hetero) Aromatic C-H Bonds using Ammonium Thiocyanate: An Overview, *J. Chem. Lett.*, **1**: 25-31 (2020).

[49] Sur I.M., Micle V., Damian G.E., Assessment of Heavy Metal Contamination and Bioremediation Potential of Thiobacillus Ferrooxidans in Soils Around Copper Quarry, *J. Environ. Prot. Ecol.*, **21(1)**: 56-62 (2020).

[50] Shajari N., Yahyaei H., Ramazani A., Experimental and Computational Investigations of Some New Cabamothioate Compounds, *Chem. Rev. Lett.*, **4**: 21-29 (2021).

[51] Majedi S., Majedi S., Existing Drugs as Treatment Options for COVID-19: A Brief Survey of Some Recent Results, *J. Chem. Lett.*, **1**: 2-8 (2020).

[52] Jalali Sarvestani M. R., Majedi S., A DFT Study on the Interaction of Alprazolam with Fullerene (C20), *J. Chem. Lett.*, **1**: 32-38 (2020).

[53] Kamel M., Mohammadifard K., Thermodynamic and Reactivity Descriptors Studies on the Interaction of Flutamide Anticancer Drug with Nucleobases: A Computational View, *Chem. Rev. Lett.*, **4**: 54-65 (2021).

[54] Majedi S., Behmagham F., Vakili M., Theoretical View on Interaction between Boron Nitride Nanostructures and Some Drugs, *J. Chem. Lett.*, **1**: 19-24 (2020)

[55] Zha TH., Castillo O., Jahanshahi H., Yusuf A., Alassafi MO., Alsaadi FE., Chu YM., A Fuzzy-Based Strategy to Suppress the Novel Coronavirus (2019-NCOV) Massive Outbreak, *Applied and Computational Mathematics*, **20**: 160-176 (2020).

[56] Zhao T., Wang M., Chu Y., On the Bounds of the Perimeter of an Ellipse, *Acta Mathematica Scientia*, **42(2)**: 491-501 (2022).

[57] Zhao T.H., Wang M.K., Hai G.J., Chu Y.M., Landen inequalities for Gaussian hypergeometric function. Revista de la Real Academia de Ciencias Exactas, Físicas y Naturales, *Serie A. Matemáticas*, **116(1)**: 1-23 (2022).

[57] Nazeer M., Hussain F., Khan MI., El-Zahar E.R., Chu Y.M., Malik M.Y., Theoretical Study of MHD Electro-Osmotically Flow of Third-Grade Fluid in Micro Channel, *Applied Mathematics and Computation*, **420**: 126868 (2022).

[58] Chu Y.M., Shankaralingappa B.M., Gireesha B.J., Alzahrani F., Khan M.I., Khan S.U., Combined Impact of Cattaneo-Christov Double Diffusion and Radiative Heat Flux on Bio-Convective Flow of Maxwell Liquid Configured by a Stretched Nano-Material Surface, *Applied Mathematics and Computation*, **419**: 126883 (2022).

[59] Zhao T.H., Khan M.I., Chu Y.M., Artificial Neural Networking (ANN) Analysis for Heat and Entropy Generation in Flow of Non-Newtonian Fluid Between Two Rotating Disks, *Mathematical Methods in the Applied Sciences*, (2021).

[60] Iqbal M.A., Wang Y., Miah M.M., Osman M.S., Study on Date–Jimbo–Kashiwara–Miwa Equation with Conformable Derivative Dependent on Time Parameter to Find the Exact Dynamic Wave Solutions, *Fractal and Fractional*, **6(1)**: 4 (2021).

[61] Zhao T.H., He Z.Y., Chu Y.M., Sharp Bounds for the Weighted Hölder Mean of the Zero-Balanced Generalized Complete Elliptic Integrals, *Computational Methods and Function Theory*, **21(3)**: 413-426 (2021).

[62] Zhao T.H., Wang M.K., Chu Y.M., Concavity and Bounds Involving Generalized Elliptic Integral of the First Kind, *J. Math. Inequal.*, **15(2)**: 701-724 (2021).

[63] Zhao T.H., Wang M.K., Chu Y.M., Monotonicity and Convexity Involving Generalized Elliptic Integral of the First Kind. Revista De La Real Academia De Ciencias Exactas, *Físicas y Naturales. Serie A. Matemáticas*, **115(2)**:1-3 (2021).

[64] Chu H.H., Zhao T.H., Chu Y.M., Sharp Bounds for the Toader Mean of order 3 in Terms of Arithmetic, Quadratic and Contraharmonic Means, *Mathematica Slovaca*, **70(5)**: 1097-112 (2020).

[65] Zhao T.H., He Z.Y., Chu Y.M., On some Refinements for Inequalities Involving Zero-Balanced Hypergeometric Function, *AIMS Math*., **5(6)**: 6479-95 (2020).

[66] Zhao T.H., Wang M.K., Chu Y.M., A Sharp Double Inequality Involving Generalized Complete Elliptic Integral of the First Kind, *AIMS Math.*, **5(5)**:4512-28 (2020).

[67] Zhao T.H., Shi L., Chu Y.M., Convexity and Concavity of the Modified Bessel Functions of the First Kind with Respect to Hölder Means, *Revista de la Real Academia de Ciencias Exactas, Físicas y Naturales. Serie A. Matemáticas*, **114(2)**:1-4 (2020).

[68] Zhao T., Wu Q., Li S., Guo R., Dian S., Jia H., Optimization Design of General Type-2 Fuzzy Logic Controllers for an Uncertain Power-Line Inspection Robot, *Journal of Intelligent & Fuzzy Systems*, **37(2)**:2203-2214 (2019).

[69] Zhao T.H., Wang M.K., Zhang W., Chu Y.M., Quadratic Transformation Inequalities for Gaussian Hypergeometric Function, *Journal of Inequalities and Applications*, **2018(1)**:1-5 (2018).

[70] Chu Y.M., Zhao T.H., Concavity of the Error Function with Respect to Hölder Means, *Math. Inequal. Appl.*, **19(2)**:589-595 (2016).

[71] Song Y.Q., Zhao T.H., Chu Y.M., Zhang X.H., Optimal Evaluation of a Toader-Type Mean by Power Mean, *Journal of Inequalities and Applications*, **2015(1)**: 1-2 (2015).

[72] Zhao T.H., Shen Z.H., Chu Y.M., Sharp Power Mean Bounds for the Lemniscate Type Means. Revista de la Real Academia de Ciencias Exactas, Físicas y Naturales, *Serie A. Matemáticas*, **115(4)**: 1-6 (2021).

[73] Chu Y.M., Zhao T.H., Convexity and Concavity of the Complete Elliptic Integrals with Respect to Lehmer Mean, *Journal of Inequalities and Applications*, **2015(1)**:1-6 (2015).

[74] Zhao T.H., Yang Z.H., Chu Y.M., Monotonicity Properties of a Function Involving the Psi Function with Applications, *Journal of Inequalities and Applications*, **2015(1)**:1-0 (2015).

[75] Chu Y.M., Wang H., Zhao T.H., Sharp bounds for the Neuman Mean in Terms of the Quadratic and Second Seiffert Means, *Journal of Inequalities and Applications*, **2014(1)**:1-4 (2014).

[76] Sun H., Zhao T.H., Chu Y.M., Liu B.Y., A Note on the Neuman-Sándor Mean, *J. Math. Inequal.*, **8(2)**: 287-297 (2014).

[77] Chu Y.M., Zhao T.H., Liu B.Y., Optimal Bounds For Neuman-Sándor Mean in Terms of the Convex Combination of Logarithmic and Quadratic or Contra-Harmonic Means, *J. Math. Inequal*., **8(2)**: 201-17 (2014).

[78] Yuming C.H., Tiehong Z.H., Yingqing S.O., Sharp Bounds for Neuman-Sándor Mean in Terms of the Convex Combination of Quadratic and First Seiffert Means, *Acta Mathematica Scientia*, **34(3)**: 797-806 (2014).

[79] Zhao T.H., Chu Y.M., Jiang Y.L., Li Y.M., Best Possible Bounds for Neuman-Sándor Mean by the Identric, Quadratic and Contraharmonic Means, *Abstract and Applied Analysis*, 2013 (2013).

[80] Zhao T.H., Chu Y.M., Liu B.Y., Optimal Bounds for Neuman-Sándor Mean in Terms of the Convex Combinations of Harmonic, Geometric, Quadratic, and Contraharmonic Means, *Abstract and Applied Analysis*, 2012 (2012).

[81] Wang M.K., Hong M.Y., Xu Y.F., Shen Z.H., Chu Y.M., Inequalities for Generalized Trigonometric and Hyperbolic Functions with one Parameter, *J. Math. Inequal.*, **14(1)**:1-21 (2020).

[82] Xu HZ., Qian WM., Chu YM., Sharp Bounds for the Lemniscatic Mean by the One-Parameter Geometric and Quadratic Means, *Revista de la Real Academia de Ciencias Exactas, Físicas y Naturales. Serie A. Matemáticas*, **116(1)**: 1-5 (2022).

[83] Karthikeyan K., Karthikeyan P., Baskonus HM, Venkatachalam K., Chu YM., Almost Sectorial Operators on Ψ-Hilfer Derivative Fractional Impulsive Integro-Differential Equations, *Mathematical Methods in the Applied Sciences*, (2021).

[84] Chu Y.M., Nazir U., Sohail M., Selim M.M., Lee J.R., Enhancement in thermal energy and solute particles using hybrid nanoparticles by engaging activation energy and chemical reaction over a parabolic surface via finite element approach. Fractal and Fractional. 5(3):119 (2021).

[85] Rashid S., Sultana S., Karaca Y., Khalid A., Chu Y.M.. Some Further Extensions Considering Discrete Proportional Fractional Operators, *Fractals*, **30(01)**: 2240026 (2022).

[86] Zhao T.H., Qian WM., Chu Y.M., Sharp Power Mean Bounds for the Tangent and Hyperbolic Sine Means, *Journal of Mathematical Inequalities*, **15(4)**: 1459-1472 (2021).

[87] Zhao T.H., Qian W.M., Chu Y.M., On Approximating the Arc Lemniscate Functions, *Indian Journal of Pure and Applied Mathematics*, **14**: 1-4 (2021).

[88] Hajiseyedazizi S.N., Samei M.E., Alzabut J., Chu Y.M., On Multi-Step Methods for Singular Fractional Q-Integro-Differential Equations, *Open Mathematics*, **19(1)**:1378-1405 (2021).

[89] He Z.Y., Abbes A., Jahanshahi H., Alotaibi N.D., Wang Y., Fractional-Order Discrete-Time SIR Epidemic Model with Vaccination: Chaos and Complexity, *Mathematics*, **10(2)**:165 (2022).

[90] Jin F., Qian ZS., Chu YM., ur Rahman M., On Nonlinear Evolution Model for Drinking Behavior under Caputo-Fabrizio Derivative, *Journal of Applied Analysis & Computation*, **12(2)**:790-806 (2022).

[91] Rashid S., Abouelmagd E.I., Khalid A., Farooq F.B., Chu Y.M., Some Recent Developments on Dynamical H-Discrete Fractional Type Inequalities in the Frame of Nonsingular and Nonlocal Kernels, *Fractals*, **30(2)**:2240110 (2022).

[92] He Z.Y., Abbes A., Jahanshahi H., Alotaibi N.D., Wang Y., Fractional-Order Discrete-Time SIR Epidemic Model with Vaccination: Chaos and Complexity, *Mathematics*. **10(2)**:165 (2022).

[93] Wang F., Khan M.N., Ahmad I., Ahmad H., Abu-Zinadah H., Chu YM., Numerical Solution of Traveling Waves in Chemical Kinetics: Time-Fractional Fishers Equations, *Fractals*, **30(02)**: 2240051 (2022).

[94] Fani M., Norouzi N., Ramezani M., Energy, Exergy, and Exergoeconomic Analysis of Solar Thermal Power Plant Hybrid with Designed PCM Storage, *International Journal of Air-Conditioning and Refrigeration*, **28(04)**: 2050030 (2020).

[95] Norouzi N., 4E Analysis of a Fuel Cell and Gas Turbine Hybrid Energy System, *Biointerface Res. Appl. Chem.*, **11**: 7568-7579 (2021).

[96] Norouzi N., Talebi S., Najafi P., Thermal-Hydraulic Efficiency of a Modular Reactor Power Plant by Using the Second Law of Thermodynamic, *Annals of Nuclear Energy*, **151**:107936 (2021).

[97] Norouzi N., Kalantari G., Talebi S., Combination of Renewable Energy in the Refinery, with Carbon Emissions Approach, *Biointerface Res. Appl. Chem.*, **10(4)**: 5780-5786 (2020).

[98] Norouzi N., Talebi S., Fabi M., Khajehpour H., Heavy Oil Thermal Conversion and Refinement to the Green Petroleum: A Petrochemical Refinement Plant Using the Sustainable Formic Acid for the Process, *Biointerface Res. Appl. Chem.*, **10(5)**: 6088-6100 (2020).

[99] Khajehpour H., Norouzi N., Bashash Jafarabadi Z., Valizadeh G., Hemmati M.H., Energy, Exergy, and Exergoeconomic (3E) Analysis of Gas Liquefaction and Gas Associated Liquids Recovery Co-Process Based on the Mixed Fluid Cascade Refrigeration Systems, *Iranian Journal of Chemistry and Chemical Engineering (IJCCE)*, (2021).

[100] Rabipour S., Perceived Stress Levels of Medical and Non-Medical Staff in the Face of COVID-19, In Mental Health and Wellness in Healthcare Workers: Identifying Risks, Prevention, and Treatment (pp. 24-33). IGI Global (2022).

[101] Rabipour S., Norouzi, N., Relationship Between Governance Quality and Public Health in the Light of Covid-19 Pandemic Control: A Case Study for Southwest Asian Countries, In Handbook of Research on SDGs for Economic Development, Social Development, and Environmental Protection. IGI Global (2022).

[102] Norouzi, N., Rabipour S., Impacts of Pollutants in Different Sectors of the Economy on Health Care Expenditures, In Handbook of Research on SDGs for Economic Development, Social Development, and Environmental Protection. IGI Global (2022).

[102] Norouzi, N., Rabipour S., An Analysis of the Health Economic Impacts of COVID-19 and Government Financial Packages in Its Management, In Handbook of Research on Building Inclusive Global Knowledge Societies for Sustainable Development. IGI Global (2022).

[103] Khajehpour H., Norouzi N., Fani M., An Exergetic Model for the Ambient Air Temperature Impacts on the Combined Power Plants and its Management Using the Genetic Algorithm, *International Journal of Air-Conditioning and Refrigeration*, **29(01)**: 2150008 (2021).

[104] Norouzi N., Talebi S., Fani M., Khajehpour H., Exergy and Exergoeconomic Analysis of Hydrogen and Power Cogeneration Using an HTR Plant, *Nuclear Engineering and Technology*, **53(8)**: 2753-2760 (2021).

[105] Norouzi N., Hosseinpour M., Talebi S., Fani M., A 4E Analysis of Renewable Formic Acid Synthesis from the Electrochemical Reduction of Carbon Dioxide and Water: Studying Impacts of the Anolyte Material on the Performance of the Process, *Journal of Cleaner Production*, **293**:126149 (2021).

[106] Liu M., Li C., Cao C., Wang L., Li X., Che J., Yang H., Zhang X., Zhao H., He G., Liu X., Walnut Fruit Processing Equipment: Academic Insights and Perspectives, *Food Engineering Reviews*, **13(4)**: 822-57 (2021).

[107] Wang Y., Li C., Zhang Y., Yang M., Li B., Dong L., Wang J., Processing Characteristics of Vegetable Oil-Based Nanofluid MQL for Grinding Different Workpiece Materials, *International Journal of Precision Engineering and Manufacturing-Green Technology*, **5(2)**: 327-339 (2018).

[108] Qiu PL., Liu SY., Bradshaw M., Rooney-Latham S., Takamatsu S., Bulgakov TS., Tang SR., Feng J., Jin DN., Aroge T., Li Y., Multi-Locus Phylogeny and Taxonomy of an Unresolved, Heterogeneous Species Complex Within the Genus Golovinomyces (Ascomycota, Erysiphales), Including G. Ambrosiae, G. Circumfusus and G. Spadiceus, *BMC Microbiology*, **20(1)**:1-6 (2020).

[109] Yang Y., Gong Y., Li C., Wen X., Sun J., Mechanical Performance of 316 L Stainless Steel by Hybrid Directed Energy Deposition and Thermal Milling Process, *Journal of Materials Processing Technology*, **291**: 117023 (2021).

[108] Li H., Zhang Y., Li C., Zhou Z., Nie X., Chen Y., Cao H., Liu B., Zhang N., Said Z., Debnath S., Extreme Pressure and Antiwear Additives for Lubricant: Academic Insights and Perspectives, *The International Journal of Advanced Manufacturing Technology*, **30**:1-27 (2022).

[109] Jia D., Zhang Y., Li C., Yang M., Gao T., Said Z., Sharma S., Lubrication-Enhanced Mechanisms of Titanium Alloy Grinding Using Lecithin Biolubricant, *Tribology International*, **169**: 107461 (2022).

[110] Zhang N., Jiao B., Ye Y., Kong Y., Du X., Liu R., Cong B., Yu L., Jia S., Jia K., Embedded Cooling Method with Configurability and Replaceability For Multi-Chip Electronic Devices, *Energy Conversion and Management*, **253**:115124 (2022).

[111] Ye Y., Jiao B., Kong Y., Liu R., Du X., Jia K., Yun S., Chen D., Experimental Investigations on the Thermal Superposition Effect of Multiple Hotspots for Embedded Microfluidic Cooling, *Applied Thermal Engineering*, **202**: 117849 (2022).

[112] Sun D., Huo J., Chen H., Dong Z., Ren R., Experimental Study of Fretting Fatigue In Dovetail Assembly Considering Temperature Effect Based on Damage Mechanics Method, *Engineering Failure Analysis*, **131**: 105812 (2022).

[113] Yang Y., Wang Y., Zheng C., Lin H., Xu R., Zhu H., Bao L., Xu X., Lanthanum Carbonate Grafted ZSM-5 for Superior Phosphate Uptake: Investigation of the Growth and Adsorption Mechanism, *Chemical Engineering Journal*, **430**:133166 (2022).

[114] Liu H., Wang Y., Li Q., Yang N., Wang Z., Wang Q., Research on the Evolution Characteristics of Oxygen-Containing Functional Groups During the Combustion Process of the Torrefied Corn Stalk, *Biomass and Bioenergy*, **158**: 106343 (2022).

[115] Fan S., Wang Y., Cao S., Sun T., Liu P., A Novel Method for Analyzing the Effect of Dust Accumulation on Energy Efficiency Loss in Photovoltaic (PV) System, *Energy*, **234**: 121112 (2021).

[116] Liu H., Li X., Ma Z., Sun M., Li M., Zhang Z., Zhang L., Tang Z., Yao Y., Huang B., Guo S., Atomically Dispersed Cu Catalyst for Efficient Chemoselective Hydrogenation Reaction, *Nano Letters*, **21(24)**: 10284-10291 (2021).

[117] Wu H., Zhang F., Zhang Z., Fundamental Spray Characteristics of Air-Assisted Injection System Using Aviation Kerosene, *Fuel*, **286**:119420 (2021).

[118] Molla MA., Furukawa M., Tateishi I., Katsumata H., Suzuki T., Kaneco S., Photocatalytic Degradation of Fenitrothion in Water with TiO2 under Solar Irradiation, *Water Conservation & Management (WCM)*, **2(2)**: 1-5 (2018).

[119] Syafiqah I., Yussof HW., The Use of Factorial Design for Analysis of Mercury Removal Efficiency Using Palm Oil Fuel Ash, *Water Conservation and Management*, **2(1)**: 10-12 (2018).